



This discussion paper is/has been under review for the journal Atmospheric Chemistry and Physics (ACP). Please refer to the corresponding final paper in ACP if available.

Comparing the CarbonTracker and TM5-4DVar data assimilation systems for CO₂ surface flux inversions

A. Babenhauserheide¹, S. Basu^{2,*}, S. Houweling², W. Peters^{3,4}, and A. Butz¹

¹IMK-ASF, Karlsruhe Institute of Technology (KIT), Karlsruhe, Germany

²Netherlands Institute of Space Research (SRON), Utrecht, the Netherlands

³Dept. of Meteorology and Air Quality, Environmental Sciences Group Wageningen University, Wageningen, the Netherlands

⁴Univ. of Groningen, Centre for Isotope Research, Groningen, the Netherlands

* now at: Earth System Research Laboratory, Global Monitoring Division, National Oceanic and Atmospheric Administration, Boulder, Colorado, USA

Received: 20 February 2015 – Accepted: 9 March 2015 – Published: 25 March 2015

Correspondence to: A. Babenhauserheide (arne.babenhauserheide@kit.edu)

Published by Copernicus Publications on behalf of the European Geosciences Union.

Title Page

Abstract

Introduction

Conclusions

References

Tables

Figures



Back

Close

Full Screen / Esc

Printer-friendly Version

Interactive Discussion



Abstract

Data assimilation systems allow for estimating surface fluxes of greenhouse gases from atmospheric concentration measurements. Good knowledge about fluxes is essential to understand how climate change affects ecosystems and to characterize feedback mechanisms. Based on assimilation of more than one year of atmospheric in-situ concentration measurements, we compare the performance of two established data assimilation models, CarbonTracker and TM5-4DVar, for CO₂ flux estimation. CarbonTracker uses an Ensemble Kalman Filter method to optimize fluxes on ecoregions. TM5-4DVar employs a 4-D variational method and optimizes fluxes on a 6° × 4° longitude/latitude grid. Harmonizing the input data allows analyzing the strengths and weaknesses of the two approaches by direct comparison of the modelled concentrations and the estimated fluxes. We further assess the sensitivity of the two approaches to the density of observations and operational parameters such as temporal and spatial correlation lengths.

Our results show that both models provide optimized CO₂ concentration fields of similar quality. In Antarctica CarbonTracker underestimates the wintertime CO₂ concentrations, since its 5-week assimilation window does not allow for adjusting the far-away surface fluxes in response to the detected concentration mismatch. Flux estimates by CarbonTracker and TM5-4DVar are consistent and robust for regions with good observation coverage, regions with low observation coverage reveal significant differences. In South America, the fluxes estimated by TM5-4DVar suffer from limited representativeness of the few observations. For the North American continent, mimicking the historical increase of measurement network density shows improving agreement between CarbonTracker and TM5-4DVar flux estimates for increasing observation density.

ACPD

15, 8883–8932, 2015

CarbonTracker and TM5-4DVar

A. Babenhauserheide
et al.

Title Page

Abstract

Introduction

Conclusions

References

Tables

Figures



Back

Close

Full Screen / Esc

Printer-friendly Version

Interactive Discussion



1 Introduction

Sources and sinks of atmospheric carbon dioxide (CO₂) largely control future climate change (Schimel, 2007). Anthropogenic emissions release roughly 10 Gt carbon into the atmosphere per year (Peters et al., 2013), part of which gets taken up by the biosphere and the oceans. The fraction of emitted CO₂ which remains in the atmosphere is the largest driver of climate change (Stocker et al., 2013, chapter 8.5.1), but the distribution and strength of carbon sources and sinks on the surface is hard to measure directly. Methods for observing the fluxes directly require either eddy covariance measurements at multiple height levels (Foken et al., 2012) or measurements of concentration changes in a sealed volume of air. But such bottom-up approaches are only representative for a given collection of vegetation types in a limited geographic area.

Inverse modelling therefore uses CO₂ concentration gradients observed in the Earth's atmosphere to quantify the spatio-temporal distribution of the net CO₂ surface fluxes (e.g. Enting, 2000; Peters et al., 2007; Chevallier et al., 2010; Feng et al., 2011; Peylin et al., 2013). To this end, various data assimilation (DA) techniques have been developed. These DA approaches differ in four main characteristics: first, they ingest different observational constraints, for example in-situ concentration measurements at different sites. Second, they represent sources and sinks of carbon differently, for example by binning them by by vegetation type or on a latitude/longitude grid. Third, they relate sources and sinks to observed atmospheric abundances using different air-mass transport models. And fourth, they use different inverse methods that find the best estimate of the source-sink distribution using the transport model, the observational constraints, the representation of sources and sinks and a prior estimate of the sources and sinks.

There are two main classes of assimilation techniques for complex inversions, variational methods and ensemble methods (Lahoz et al., 2007; Lahoz and Schneider, 2014). Both approaches are approximate variants of the general Bayesian optimal estimation scheme (e.g. Rodgers, 2000) which aims at balancing prior or background in-

Title Page

Abstract

Introduction

Conclusions

References

Tables

Figures



Back

Close

Full Screen / Esc

Printer-friendly Version

Interactive Discussion



observations. Building on these results, Sect. 5 analyzes the estimated surface fluxes and tests their sensitivity to observation density.

2 Inverse methods and model setup

The DA systems aim at inferring a state vector \mathbf{x} that contains spatially and temporally binned surface fluxes or a related quantity such as scaling factors for an initial guess flux field. To this end, the systems exploit measurements of the atmospheric concentration chained into an observation vector \mathbf{y} . Fluxes and measured concentrations are linked through the transport and observation operator \mathbf{H} which is linear for the case of our CO₂ flux inversions, but in general could be non-linear such as for CH₄ flux inversions. Typically, the inverse problem of estimating \mathbf{x} from a set of observations \mathbf{y} is ill posed. Due to sparse observational coverage, measurement errors or measurement configuration, the observations contain insufficient information to determine all components of \mathbf{x} independently. A background flux estimate \mathbf{x}_b from biosphere and ocean models is used to provide a constraint that fills the null-space where measurement information is insufficient. Accordingly, the state vector of fluxes \mathbf{x} is determined by minimizing a cost function J that typically consists of two terms, the mismatch between measured and modelled observations and the mismatch between the fluxes to be estimated and the background estimate,

$$J = (\mathbf{y} - \mathbf{H}\mathbf{x})^T \mathbf{R}^{-1} (\mathbf{y} - \mathbf{H}\mathbf{x}) + (\mathbf{x} - \mathbf{x}_b)^T \mathbf{B}^{-1} (\mathbf{x} - \mathbf{x}_b) \quad (1)$$

with \mathbf{R} the observation covariance and \mathbf{B} the background flux covariance. \mathbf{R} and \mathbf{B} define the relative weights of the measurement and background mismatch.

Title Page

Abstract

Introduction

Conclusions

References

Tables

Figures



Back

Close

Full Screen / Esc

Printer-friendly Version

Interactive Discussion



In general, minimization of Eq. (1) can be solved by means of matrix algebra (Rodgers, 2000) yielding optimized fluxes and their error covariances,

$$\hat{\mathbf{x}} = \mathbf{x}_b + \mathbf{B}\mathbf{H}^T(\mathbf{H}\mathbf{B}\mathbf{H}^T + \mathbf{R})^{-1}(\mathbf{y} - \mathbf{H}\mathbf{x}_b) \quad (2)$$

$$= \mathbf{x}_b + (\mathbf{H}^T\mathbf{R}^{-1}\mathbf{H} + \mathbf{B}^{-1})^{-1}\mathbf{H}^T\mathbf{R}^{-1}(\mathbf{y} - \mathbf{H}\mathbf{x}_b), \quad (3)$$

$$\hat{\mathbf{B}} = \mathbf{B} - \mathbf{B}\mathbf{H}^T(\mathbf{H}\mathbf{B}\mathbf{H}^T + \mathbf{R})^{-1}\mathbf{H}\mathbf{B} \quad (4)$$

$$= (\mathbf{H}^T\mathbf{R}^{-1}\mathbf{H} + \mathbf{B}^{-1})^{-1}, \quad (5)$$

with $\hat{\mathbf{x}}$ the a posteriori state vector and $\hat{\mathbf{B}}$ as the respective covariance matrix. Equivalence of equation pairs – Eqs. (2) and (3), Eqs. (4) and (5) – can be shown (Rodgers, 2000, Eqs. 4.11 and 2.27).

While theoretically the minimization of Eq. (1) reduces to a matrix inversion for linear systems like CO₂ flux inversion (e.g. Rodgers, 2000), the large number of parameters to be estimated and the amount of measurements to be ingested requires approximate methods such as EnSRF and 4DVar which are numerically efficient.

2.1 CarbonTracker: EnSRF based data assimilation

CarbonTracker is an inverse modelling framework based on the Ensemble Square Root Filter (EnSRF) developed by Peters et al. (2005). Instead of solving the minimization problem in one step, the EnSRF determines optimized surface fluxes sequentially in a time stepping approach with \mathbf{x}_t defining a subset of \mathbf{x} for a certain time window. In our standard setup \mathbf{x} contains scaling factors for the surface fluxes for 96 weeks, while \mathbf{x}_t only spans 5 weeks.

Commonly, a gain matrix \mathbf{G} is defined as

$$\mathbf{G} = \mathbf{B}\mathbf{H}^T(\mathbf{H}\mathbf{B}\mathbf{H}^T + \mathbf{R})^{-1} \quad (6)$$

$$= (\mathbf{H}^T\mathbf{R}^{-1}\mathbf{H} + \mathbf{B}^{-1})^{-1}\mathbf{H}^T\mathbf{R}^{-1}. \quad (7)$$

Equations (2) and (4) then read

$$\hat{\mathbf{x}}_t = \mathbf{x}_{b,t} + \mathbf{G}_t (\mathbf{y}_t - \mathbf{H}_t \mathbf{x}_{b,t}), \quad (8)$$

$$\hat{\mathbf{B}}_t = \mathbf{B}_t - \mathbf{G}_t \mathbf{H}_t \mathbf{B}_t \quad (9)$$

with the Gain Matrix

$$\mathbf{G}_t = \mathbf{B}_t \mathbf{H}_t^T (\mathbf{H}_t \mathbf{B}_t \mathbf{H}_t^T + \mathbf{R}_t)^{-1} \quad (10)$$

where subscript t indicates quantities of reduced dimensions, for the time step under investigation. Once Eqs. (8) and (9) are solved for time slice t , the solution of the scaling factors $\hat{\mathbf{x}}_t$ is used as the background estimate $\mathbf{x}_{b,t+1}$ for the next time slice $t+1$, assuming that a simple persistence forecast is adequate for our CO₂ flux inversion problem,

$$\mathbf{x}_{b,t+1} = \hat{\mathbf{x}}_t. \quad (11)$$

The covariance \mathbf{B}_{t+1} is prescribed at each time step as described in Peters et al. (2005). Given an initial guess for the first background state, this strategy allows for sequentially calculating the complete state vector $\hat{\mathbf{x}}$.

To estimate the gain matrix \mathbf{G}_t , the EnSRF uses an ensemble approach. The ensemble members $\mathbf{x}_{b,t}^i = \mathbf{x}_{b,t} + \Delta \mathbf{x}_{b,t}^i$ ($i = 1 \dots E$) of the background state are drawn such that their mean and covariance is consistent with the background state $\mathbf{x}_{b,t}$ and background covariance \mathbf{B}_t , respectively, so that

$$\mathbf{B}_t \approx \frac{1}{E-1} \left(\Delta \mathbf{x}_{b,t}^1, \Delta \mathbf{x}_{b,t}^2, \dots, \Delta \mathbf{x}_{b,t}^E \right) \cdot \left(\Delta \mathbf{x}_{b,t}^1, \Delta \mathbf{x}_{b,t}^2, \dots, \Delta \mathbf{x}_{b,t}^E \right)^T \quad (12)$$

Title Page

Abstract

Introduction

Conclusions

References

Tables

Figures



Back

Close

Full Screen / Esc

Printer-friendly Version

Interactive Discussion



Then, the terms $H_t B_t H_t^T$ and $B_t H_t^T$ required for calculating G_t following Eq. (10) can be approximated using the results from an ensemble run of the possibly non-linearized transport model \mathcal{H}

$$H_t B_t H_t^T \approx \frac{1}{E-1} \left(\mathcal{H}_t \Delta x_{b,t}^1, \mathcal{H}_t \Delta x_{b,t}^2, \dots, \mathcal{H}_t \Delta x_{b,t}^E \right) \cdot \left(\mathcal{H}_t \Delta x_{b,t}^1, \mathcal{H}_t \Delta x_{b,t}^2, \dots, \mathcal{H}_t \Delta x_{b,t}^E \right)^T \quad (13)$$

$$B_t H_t^T \approx \frac{1}{E-1} \left(\Delta x_{b,t}^1, \Delta x_{b,t}^2, \dots, \Delta x_{b,t}^E \right) \cdot \left(\mathcal{H}_t \Delta x_{b,t}^1, \mathcal{H}_t \Delta x_{b,t}^2, \dots, \mathcal{H}_t \Delta x_{b,t}^2 \right)^T, \quad (14)$$

where the approximation becomes more exact with increasing ensemble size E . The EnSRF method yields robust results with non-linear transport operators \mathcal{H} as long as the transport model is close to linear for small perturbations ($\mathcal{H}(x + \Delta x) \approx Hx + H\Delta x$). Using Eqs. (13) and (14), the gain matrix G_t can be calculated from Eq. (10), finally to update the state estimate \hat{x}_t via Eq. (8). Peters et al. (2005) describe in detail how to estimate the state covariance \hat{B}_t by separately updating the ensemble deviations $\Delta x_{b,t}^j$ while avoiding the costly evaluation of Eq. (10) and circumventing spurious underestimation of \hat{B}_t . Overall, CarbonTracker's EnSRF approach requires running the transport model \mathcal{H} for E ensemble members over the time period covered by all time steps t . At each time step t the transport model is sampled at all measurement instances within the time step and the above methodology is followed.

CarbonTracker uses a refined approach for stepping through the entire time period considered. CarbonTracker's state vector x_t is subdivided into five one-week bins (five cycles) resulting in an assimilation window of five weeks (Peters et al., 2005, chapter 2.3). At each optimization step the oldest cycle at the "end" of the state vector drops out of the state vector and is used as a posteriori flux estimate while a new cycle is added to the "beginning" of the state vector according to Eq. (11). As such, each one-week

Title Page

Abstract

Introduction

Conclusions

References

Tables

Figures

◀

▶

◀

▶

Back

Close

Full Screen / Esc

Printer-friendly Version

Interactive Discussion



total covariance in the transcom region matches the variance in Northern Hemisphere regions. The covariance for ocean regions uses the results of the ocean inversion by Jacobson et al. (2007a). Temporal covariance in CarbonTracker stems from processing observations multiple times in the timestepping approach. The observation covariance R is assumed diagonal.

The version of CarbonTracker used here is derived from version 1.0 of the code maintained by Wageningen University with the same state vector as CarbonTracker North America (as used in Peters et al., 2007) and without a zoom region.

2.2 TM5-4DVar: variational data assimilation

Whereas the EnSRF in CarbonTracker reduces the dimension of the minimization problem of Eq. (1) by solving sequentially for time-sliced state vectors, the 4DVar method leaves the dimension of the state vector intact and instead approaches the minimum of the cost function step-by-step. The iterative minimization of Eq. (1) in TM5-4DVar is described in detail by Meirink et al. (2008). It employs the conjugate gradient algorithm (Navon and Legler, 1987) which is equivalent to the Lanczos method (Lanczos, 1950) and requires calculation of the cost function gradient

$$\nabla_{\mathbf{x}} J = \mathbf{B}^{-1}(\mathbf{x}_n - \mathbf{x}_b) - \mathbf{H}^T \mathbf{R}^{-1}(\mathbf{y} - \mathbf{H}\mathbf{x}_n) \quad (15)$$

where subscript n indicates the n th iterative step. The adjoint formulation of TM5 allows calculating the cost function gradient by a single run of the transport model and its adjoint (Errico, 1997; Chevallier et al., 2005). The conjugate gradient algorithm further provides the leading eigenvalues and eigenvectors of the preconditioned Hessian

$$\nabla_{\chi}(\nabla_{\mathbf{x}} J) = \mathbf{B}^{-1} + \mathbf{H}^T \mathbf{R}^{-1} \mathbf{H}, \quad (16)$$

which is the second derivative of the cost function J with respect to the dimensionless preconditioned state χ defined as $\mathbf{x} = \mathbf{L}\chi + \mathbf{x}_b$, where \mathbf{L} is the preconditioning matrix with $\mathbf{B} = \mathbf{L}\mathbf{L}^T$. This can be used to construct the inverse of the state covariance $\hat{\mathbf{B}}^{-1}$

Title Page

Abstract

Introduction

Conclusions

References

Tables

Figures



Back

Close

Full Screen / Esc

Printer-friendly Version

Interactive Discussion



as defined in Eq. (4). After n steps, corresponding to n runs of the forward and the adjoint model, the minimization algorithm yields an optimized state estimate $\hat{\mathbf{x}}_n$ and the first n eigenvalues λ_i ($\lambda_i > 1$) and eigenvectors \mathbf{v}_i ($i = 1, \dots, n$) for the eigensystem of the preconditioned Hessian. The latter can be used to construct an approximate error covariance matrix,

$$\hat{\mathbf{B}}_n \approx \mathbf{B} + \sum_{i=1}^n \left(\frac{1}{\lambda_i} - 1 \right) (\mathbf{L}\mathbf{v}_i)(\mathbf{L}\mathbf{v}_i)^T. \quad (17)$$

With increasing number of iterations, the optimized state vector $\hat{\mathbf{x}}_n$ approaches the optimal state vector $\hat{\mathbf{x}}$ at the minimum of the cost function and the approximate state covariance $\hat{\mathbf{B}}_n$ approaches $\hat{\mathbf{B}}$ from above (Basu et al., 2013). For practical purposes the iteration is stopped when the gradient norm reduction exceeds a threshold, i.e.

$$|\nabla_{\mathbf{x}} \mathcal{J}(\mathbf{x}_n)| \leq \eta \cdot |\nabla_{\mathbf{x}} \mathcal{J}(\mathbf{x}_0)| \quad (18)$$

with the constant chosen to be $\eta = 10^{-9}$ here.

TM5-4DVar's state vector \mathbf{x} is binned temporally in monthly fluxes and spatially on the transport model grid scale, i.e. $6^\circ \times 4^\circ$ longitude \times latitude. Fluxes are categorized into biosphere, ocean, fire and fossil fuel. To create a setup comparable to CarbonTracker, only biosphere and ocean fluxes are optimized. The background covariance \mathbf{B} of the state vector is characterized by a global temporal and spatial correlation length. By default TM5-4DVar uses an exponential decay with a temporal and spatial length scale of 1 month and 200 km for biosphere fluxes and 3 months and 1000 km for ocean fluxes. As such, the temporal binning of TM5-4DVar's state vector containing monthly bins is about a factor 4 coarser than the temporal binning of CarbonTracker's weekly bins. TM5-4DVar's spatial binning has a different overall structure. Whereas CarbonTracker's prior fluxes are fully correlated inside the 240 ecoregions and mostly uncorrelated between different ecoregions, the correlation of TM5-4DVar's fluxes exponentially falls off around each grid box. The exponential decay in TM5-4DVar's temporal background correlation limits the effects of observations in time. However, TM5-4DVar has

Title Page

Abstract

Introduction

Conclusions

References

Tables

Figures

◀

▶

◀

▶

Back

Close

Full Screen / Esc

Printer-friendly Version

Interactive Discussion



no strict limit on the time window during which observations can be linked to fluxes but rather reduces the strength of the influence with temporal lag. TM5-4DVar can adjust surface fluxes in response to any observation during the entire considered time period given that the transport model reveals a link between fluxes and observations. As for CarbonTracker, the observation covariance R is assumed diagonal.

3 Setup of the comparison

Given the setup of the CarbonTracker and TM5-4DVar modelling systems, we aim at comparing the performance of their data assimilation concepts for the purpose of CO₂ surface flux estimation when assimilating atmospheric CO₂ concentration records. To avoid affecting conclusions about the inverse methodology, care must be taken that model input such as transport parameters, background estimates, initial concentration fields and assimilated observations are harmonized as far as possible. However, as outlined in Sect. 2, conceptual differences between the models prevent us from making the model setup literally identical.

3.1 Transport model and observation operator

To connect concentration measurements and surface fluxes, CarbonTracker and TM5-4DVar use a transport model which transports the CO₂ tracer using meteorological fields. Both models use the Tracer Model 5 (TM5) as described by Krol et al. (2005) which utilizes meteorological data from the European Centre for Medium-Range Weather Forecasts (ECMWF, 2013). For CarbonTracker, we follow the setup used by Peters et al. (2007). For TM5-4DVar our setup differs from the setup used by Basu et al. (2013) in one main aspect to be consistent with CarbonTracker: the CO₂ concentration field is sampled in the second model layer (≈ 980 hPa ≈ 170 m) or higher instead of in the first model layer (≈ 994 hPa ≈ 50 m) or higher. Except for these adjustments and some minor differences due to different interfaces of the inverse methods, the ver-

Title Page

Abstract

Introduction

Conclusions

References

Tables

Figures



Back

Close

Full Screen / Esc

Printer-friendly Version

Interactive Discussion



sions of TM5 used by the CarbonTracker and TM5-4DVar systems we are using are the same.

3.2 Background flux and initial guess

CarbonTracker and TM5-4DVar use the same background fluxes and initial concentration fields. The biosphere fluxes are taken from the Simple Biosphere model using the Carnegie-Ames-Standord Approach (SIBCASA as by Schaefer et al., 2008). SIBCASA is a carbon cycle model that represents the uptake of CO₂ by different types of vegetation and its subsequent transfer back to the atmosphere through autotrophic and heterotrophic respiration. Its mechanistic description of the processes involved is driven by a combination of high-resolution weather data and satellite remote sensing products and includes interactions between the carbon, water, and energy cycles of the land-surface. For the oceans both models use Ocean Inversion Fluxes (oif), the output from an ocean inversion which assumes that the uptake of antropogenic CO₂ increases proportional to the mismatch between atmospheric and oceanic CO₂ partial pressure. Fire fluxes are taken from the Global Fire Emissions Database version 2 (GFEDv2 van der Werf et al., 2010). Fossil fuel fluxes are taken from the Miller dataset as described in Peters et al. (2007) and its Supplement.

The initial concentration field is generated from the output of a previous CarbonTracker run which ended on 1 January 2007. The field for 2009 is derived by increasing the concentration by 1.9 parts per million (ppm) per year. The value 1.9 ppm was chosen based on tests of the fit to observation sites in the first month of 2009.

The covariance of the fluxes is defined in the models as described in Sects. 2.1 and 2.2. Due to the different ways of specifying the state vector x in CarbonTracker and TM5-4DVar, it is not possible to get an exact match of the flux uncertainties. We harmonize the overall covariance by adjusting the prior flux uncertainty in TM5-4DVar to match uncertainty of a CarbonTracker run with a monthly cycle for global and continental aggregates.

CarbonTracker and TM5-4DVar

A. Babenhauserheide et al.

Title Page

Abstract

Introduction

Conclusions

References

Tables

Figures



Back

Close

Full Screen / Esc

Printer-friendly Version

Interactive Discussion



3.3 Observations and observation errors

Both DA systems use the same observations from the “obspack” compilation of in-situ CO₂ concentration measurements (Masarie et al., 2014; NOAA Environmental Sciences Division, Oak Ridge National Laboratory, 2013, version: PROTOTYPE v1.0.2 2013-01-28). Discrete (e.g. one sample per week) measurements from surface flask sites, in situ continuous (and semi-continuous) measurements from surface sites and towers, and aircraft campaign measurements are collected, aggregated and quality screened to make them suitable for inverse flux estimation. At many but not all of the continuous measurement sites, the measurements are averaged to provide afternoon or nighttime averages (depending on the type of site, e.g., continental planetary boundary layer site or mountain site), using intra-day averaging periods representative of large scale fluxes and discarding single measurements outside the respective averaging periods. For our baseline CarbonTracker and TM5-4DVar runs, we exclude 21 measurement sites from the assimilation to use them as validation sites.

Additionally we take out 5 sites which have more than 1000 measurements in the assimilation period. This is to keep the TM5-4DVar results representative of TM5-4DVar runs which use the native TM5-4DVar input. When using these 5 sites with the CarbonTracker preprocessing, TM5-4DVar shows strong gradients between neighboring grid cells in North America which it does not show when processing its native set of observations. In addition to these 26 excluded sites, there are 24 further sites from which the default run of CarbonTracker uses no data or only a subset of the observations. Reasons for not using some of the observation data of a site include that the data is assumed not representative of its grid-cell or recorded in aircraft campaigns.

Measurement uncertainty is set to a fixed value for each site accounting for the measurement errors and for representativeness errors. The latter originate from using the in-situ samples to represent the CO₂ concentration in a transport model grid box of 6° longitude and 4° latitude. Concentration uncertainties range from 0.75 ppm for marine boundary layer sites over 2.5 ppm for land sites up to 7.5 ppm for sites which experi-

Title Page

Abstract

Introduction

Conclusions

References

Tables

Figures



Back

Close

Full Screen / Esc

Printer-friendly Version

Interactive Discussion



ence variable meteorological conditions. Table 1 in the Supplement lists the observation records used in our study. Figure S1 shows the global distribution of observation sites together with a visual representation of their weight due to sampling frequency and representativeness error. In our setup CarbonTracker and TM5-4DVar use the same representativeness errors.

4 A posteriori concentration fields

As a first step, we compare and validate the performance of CarbonTracker and TM5-4DVar by evaluating the difference between measured and modelled CO₂ concentration fields at the location of various ground sampling stations. Comparing concentration fields at the assimilated sites in Sect. 4.1 provides a check to verify that data assimilation works in both systems. Comparing measured and modelled concentrations at non-assimilated sites in Sect. 4.2 demonstrates to what extent the data assimilation approaches yield improvements where observational constraints are distant in space and/or time. CarbonTracker and TM5-4DVar are both run with the baseline setup (as described in Sect. 3) for a 23 month period starting on 1 February 2009.

4.1 Assimilated sites

As an example for an assimilated site, Fig. 1 shows a time series of measured and modelled CO₂ concentrations at Mauna Loa (MLO), Hawaii, located 3399 m a.s.l. in the Pacific. For the period from 1 February 2009, to 30 December 2010, the models assimilate 94 weekly flask measurements. We compare the observations to a posteriori and a priori model concentrations. The a posteriori concentrations are sampled using the a posteriori surface fluxes estimated by CarbonTracker or TM5-4DVar. The prior model concentrations are sampled using the background (prior) flux estimate common to both models. The Mauna Loa record demonstrates that the a posteriori concentrations produced by both models match the observations within the uncertainty estimate and that

Title Page

Abstract

Introduction

Conclusions

References

Tables

Figures



Back

Close

Full Screen / Esc

Printer-friendly Version

Interactive Discussion



the match is substantially better than for the prior concentration fields. Differences between CarbonTracker and TM5-4DVar are much smaller than the representativeness error of the measurements at Mauna Loa (0.75 ppm) over the entire period. This is consistent with the results at other sites.

The mismatch between measured and modelled CO₂ concentrations for all assimilated measurements is shown in Fig. 2, with the prior concentrations, the a posteriori concentrations optimized by CarbonTracker, and the a posteriori concentrations optimized by TM5-4DVar. The concentration mismatch is normalized by the representativeness error of the observations such that a (unitless) mismatch of 1 corresponds to a mismatch with the magnitude of the representativeness error. Unlike the time series for Mauna Loa, the histograms only integrate over the 1 year period 3 April 2009 to 2 April 2010 in order to be consistent with the analysis of the a posteriori surface fluxes in Sect. 5. This time period gives the models sufficient spin-up and spin-down time, given that the initial concentration is already well-optimized by a previous CarbonTracker run.

The concentrations from the Prior Forward Run in Fig. 2 reveal an overall bias in the normalized (unitless) mismatch of 0.37 with a standard deviation of 1.09. Tentatively, the prior fields show a dipole pattern with peaks around -1 and 1 which can be traced back to the Northern Hemisphere prior generally overestimating the observations and the Southern Hemisphere prior generally underestimating the observations. The CarbonTracker and TM5-4DVar histograms show small biases of 0.006 and 0.025 with standard deviation of 0.727 and 0.650, respectively. Compared to the prior, both DA systems improve the overall bias and they substantially reduce the spread of the observation-model mismatch. Normalized standard-deviations smaller than 1 indicate that the mismatch is on average smaller than the estimated representativeness error, which points to a conservative choice of representativeness errors and consequently a stronger than optimal influence of the prior flux estimate. However, avoiding this would require using the output of the assimilation systems to adjust their input parameters which could lead to transient errors in the result.

**CarbonTracker and
TM5-4DVar**A. Babenhauserheide
et al.

Title Page

Abstract

Introduction

Conclusions

References

Tables

Figures



Back

Close

Full Screen / Esc

Printer-friendly Version

Interactive Discussion



and aircraft campaigns which provide a high number of measurements. Normalized bias and standard deviation of the prior mismatch are 0.66 and 1.03, respectively. The normalized biases of the mismatch for CarbonTracker and TM5-4DVar are 0.097 and 0.004, respectively, and the standard deviation of the histograms are 0.835 and 0.839, indicating that assimilating observations with the DA systems substantially improves the match to independent data when compared to the prior performance. The spread of the a posteriori model-observation mismatch, however, is somewhat greater than for the comparison to assimilated measurements. This is as expected and indicates a slightly worse performance of both models for the non-assimilated than for assimilated sites.

4.2.1 Robustness of the result

CarbonTracker a posteriori concentrations show a larger bias for non-assimilated measurements (0.097) than for assimilated measurements (0.006). TM5-4DVar biases are more similar for non-assimilated (0.004) and assimilated measurements (0.025). In order to investigate whether these differences are likely to be an artefact of our selection of validation sites, we conduct a resampling experiment. Out of the 50 sites for which there are non-assimilated observations – our 2 validation sites, aircraft measurements and sites for which only a given measurement method is assimilated – we randomly select subsets of 25 sites and recalculate the statistical model-observation bias for non-assimilated measurements. Then we repeat the exercise 10 times and examine the distribution of the resampled CarbonTracker and TM5-4DVar biases. Figure 5 shows that the normalized biases for the CarbonTracker baseline run consistently scatter around 0.08 with a standard deviation of 0.04 while the TM5-4DVar average bias and standard deviation are -0.04 and 0.07, respectively.

So, while CarbonTracker a posteriori concentrations appear offset from the (non-assimilated) observations, TM5-4DVar does not show a significant overall bias but greater station-to-station variability for the model-observation mismatch.

CarbonTracker and TM5-4DVar

A. Babenhauserheide et al.

Title Page

Abstract

Introduction

Conclusions

References

Tables

Figures



Back

Close

Full Screen / Esc

Printer-friendly Version

Interactive Discussion



the real uncertainties due to measurement and representativeness errors. With this caveat, the sink estimates of the two models are consistent within the TM5-4DVar uncertainties and also match previous findings for CarbonTracker (Peters et al., 2007). Examining the time series of globally aggregated surface fluxes in Fig. 7 confirms that the two DA systems are consistent on the global scale, both showing stronger summer uptake than the prior.

Figure 8 illustrates the a posteriori biogenic and oceanic fluxes aggregated over the one-year time period on continental scale regions. Agreement between CarbonTracker and TM5-4DVar is found for North America, Africa, Europe, and Australia, as well as for all the oceans except for the Indian Ocean. The optimized fluxes in these regions differ by less than the yearly uncertainties estimated from TM5-4DVar's statistical error aggregation (see Basu et al., 2013). On the other hand, the modelled fluxes from CarbonTracker and TM5-4DVar differ by more than their uncertainty in South America, Asia and the Indian Ocean. In South America they differ by roughly two times the estimated uncertainty, therefore we take a more detailed look at this discrepancy.

5.1.1 TM5-4DVar's flux anomaly in South America

The time series of South American surface fluxes in Fig. 9 reveals that the flux differences in South America stem from particularly large emission estimates in summer 2009 by TM5-4DVar. The temporal structure of TM5-4DVar fluxes for the Indian Ocean as well as the Pacific Ocean, suggest that ocean uptake compensates for the large South America source to match the hemispheric flux budget.

South America suffers from sparseness of observational constraints such that validation of the estimated surface fluxes via comparison of measured and modelled atmospheric CO₂ concentrations is difficult. Aircraft measurements regularly conducted in South America do not provide deeper insight, because they have a data gap in the critical time between June and August 2009. The only other site that is close to the South America flux region is Arembepe in Brazil (ABP, 12.77° S, 38.17° W), a ground sampling station which is used as constraint within our data assimilation exercise.

Title Page

Abstract

Introduction

Conclusions

References

Tables

Figures



Back

Close

Full Screen / Esc

Printer-friendly Version

Interactive Discussion



CarbonTracker and
TM5-4DVarA. Babenhauserheide
et al.

Title Page

Abstract

Introduction

Conclusions

References

Tables

Figures



Back

Close

Full Screen / Esc

Printer-friendly Version

Interactive Discussion



To check its impact on the fluxes, we perform a sensitivity run without assimilating Arembepe. In this run both models are similarly good at matching modelled a posteriori and measured CO₂ concentrations in Arembepe and mostly follow the prior (see Fig. 10). When assimilating observations from Arembepe however, TM5-4DVar closely follows the observations in spring 2009 while CarbonTracker only moves halfway from the prior to the observations. This can be explained by the outlier-detection in CarbonTracker: when the difference between the model and a measurement is more than three times the estimated representativeness error of the measurement, CarbonTracker ignores the measurement as outlier. As marine boundary layer site, Arembepe is assigned a representativeness error of only 0.75 ppm, so CarbonTracker ignores most measurements before May 2009.

The aggregated fluxes in Fig. 8 show that assimilating the measurements in Arembepe has a significant effect on the a posteriori fluxes of TM5-4DVar. When taking out Arembepe from the baseline run, TM5-4DVar's attribution of fluxes shifts: the sinks in the Pacific and the Indian Ocean weaken while the strong source in South America disappears. The time series in Fig. 9 provide a temporal fingerprint of the flux difference due to removing Arembepe from the assimilation which identifies the changes in the Pacific and the Indian Ocean as compensation for the removal of the strong source in South America.

The flux changes in CarbonTracker with assimilating Arembepe are within the estimated uncertainties, in the yearly aggregated fluxes as well as in the time series. Disabling the outlier rejection in CarbonTracker causes the modelled concentrations to follow the observations much closer, but as shown in Fig. 9 it does not show the additional source seen in TM5-4DVar between June and August 2009 and neither the compensation fluxes TM5-4DVar gives in the oceans.

The fluxes induced by assimilating Arembepe show that TM5-4DVar is more susceptible than CarbonTracker to the effect of single measurement sites in regions with very low observation density.

5.1.2 CarbonTracker with longer assimilation window

Figure 8 shows that the difference in the Asian flux estimates is not affected by removing Arembepé from the assimilated sites. When increasing the assimilation time window of CarbonTracker to 5×20 days (“ 5×20 ”), however, CarbonTracker yields roughly the same aggregated flux as TM5-4DVar.

The time series in Fig. 11 suggests that the change in the CarbonTracker estimate of Asian fluxes when going to the longer assimilation window originates from high frequency corrections to the prior fluxes. If the biosphere model needs to be corrected for only one week, the run with weekly flux bins can adjust that week separately while the run with 20 day flux bins has to adjust a full 20 day period. To test this theory, we verified that a run with an assimilation window consisting of ten one-week cycles yields a similar Asian sink as the run with five one-week cycles (1.84 instead of 1.61 Pg C a^{-1}) which does not increase further when going to fifteen one-week cycles (not shown), while a run with three 20 day cycles yields a similar Asian sink as the run with five 20 day cycles (2.22 instead of 2.25 Pg C a^{-1}).

For a quantitative discussion of the propagation of aggregation errors see Turner and Jacob (2015). Our findings suggest that there is an impact of roughly 0.5 Pg C a^{-1} from high frequency mismatches between the prior model and the measured concentrations during the Asian summer which cannot be corrected accurately with a binsize of 20 days or more.

In summary we see good agreement for the baseline fluxes between CarbonTracker and TM5-4DVar on a global scale and for most continents and oceans. The mismatch of the fluxes in South America, the Indian Ocean and Asia can be traced back to two distinct effects: a different flux response in regions with very limited observation coverage and using weekly (CarbonTracker) or monthly (TM5-4DVar) adjustments to account for mismatches on shorter time scales.

Title Page

Abstract

Introduction

Conclusions

References

Tables

Figures



Back

Close

Full Screen / Esc

Printer-friendly Version

Interactive Discussion



5.2 Sensitivity to observation coverage

In order to assess the importance of data density and coverage on the two DA systems, we follow the approach which Bruhwiler et al. (2011) used to analyze the performance of their initial version of a fixed-lag Ensemble Kalman Smoother (Bruhwiler et al., 2005). We carry out 5 “historical” model-runs where we stepwise increase the number of assimilated observation sites, mostly following the historical availability of data. The first run, termed “2/cont”, assimilates observations from up to 2 stations per continent. It represents an extremely sparse observation network with different sampling frequencies per site. The runs “1988” and “2000” assimilate observations from all sites that were active in the years 1988 and 2000, respectively. The “2000” run assimilates roughly the same number of observations as our baseline run. The run “2010” uses all stations which were active in the year 2010 except for Arembepe. We exclude Arembepe from the “2010” run, because as shown in Sect. 5.1 the different treatment of the observations there would dominate the flux changes and as such mask other effects. Figure S2 illustrates the observation density and coverage for the different historical runs while Table S1 lists the sites included for all the historical runs.

Figure 12 shows the globally aggregated prior and a posteriori fluxes for the baseline setup and each of the historical runs. All the historical runs for both models, CarbonTracker as well as TM5-4DVar, yield consistent estimates of the global (biospheric and oceanic) carbon sink. The results differ by a few tenths of a PgCa^{-1} which is well below the TM5-4DVar uncertainty estimate of about 1PgCa^{-1} . This consistency is expected since the global carbon sink is well constrained by the trend in global background concentrations. Compared to the prior, all runs indicate a stronger sink by more than 1PgCa^{-1} . The global flux estimate is robust against changes in the observation coverage and against the choice of the inverse model.

On the continental scale we take a closer look at North America, since changes in observation density are historically most pronounced there. Figure 13 shows that TM5-4DVar and CarbonTracker fluxes for North America become more similar the

[Title Page](#)[Abstract](#)[Introduction](#)[Conclusions](#)[References](#)[Tables](#)[Figures](#)[Back](#)[Close](#)[Full Screen / Esc](#)[Printer-friendly Version](#)[Interactive Discussion](#)

denser the observation network becomes, with almost the same flux estimate in the “2010” setup in which the models assimilate more than 15 sites on the North American continent (see Fig. 14). This good match of both models suggests that the density of observation sites in North America suffices to optimize continental scale fluxes with some degree of certainty. Separating the fluxes of the two North America Transcom regions (Fig. 13) shows that for the more homogeneous transcom region in Boreal North America the results from both models are already converged with the observation coverage in the “1988” run, while in the more heterogeneous North American Temperate region with many agricultural regions, the models only converge in the “2010” setup.

The stronger land sink seen by TM5-4DVar for “2/cont” stems from assimilating only two sites: a site in West Branch in Iowa, USA (WBI, 41.7° N, 91.4° W), in the US corn belt, and a site on Sable Islands, Nova Scotia, Canada (WSA, 43.9° N, 60.0° W). In TM5-4DVar, the strong summer sink near West Branch dominates the North America fluxes and increases the sink from roughly 1 PgCa⁻¹ in the “2010” run to more than 1.6 PgCa⁻¹ in the “2/cont” run. CarbonTracker is less susceptible to this effect than TM5-4DVar, because its ecoregion approach enforces a correlation between the fluxes for all regions in the corn belt as well as for all regions with grassland – both region-types span the area from the southern parts of North America up to the border of Canada. This makes it more likely that a potential flux adjustment is constrained by more than one site which gives it a stronger meridional coupling. Since meridional mixing is much slower than zonal mixing, stronger meridional coupling forces a larger region to change in the same way. As such the ecoregion approach makes it more likely that a potential flux adjustment is constrained by more than one site.

On the other hand, the overall North American sink of 0.65 PgCa⁻¹ estimated by CarbonTracker in the “1988” run are 30 % lower than the sink of 0.95 PgCa⁻¹ in the “2010” run, while in TM5-4DVar the “1988” and the “2010” run differ only by 10 % (0.1 PgCa⁻¹). The difference between the results for the “2000” and the “2010” runs in North America is on the order of 0.1 PgCa⁻¹ for both models, but in different directions. So with low observation coverage, the quality of the inversion in either system

CarbonTracker and
TM5-4DVarA. Babenhausenheide
et al.

Title Page

Abstract

Introduction

Conclusions

References

Tables

Figures



Back

Close

Full Screen / Esc

Printer-friendly Version

Interactive Discussion



depends on the exact distribution of the observations. This suggests that with the coverage from “2000”, we need to assume a minimum uncertainty of 0.25 PgCa^{-1} from only the choice of the inverse method. For “2010” this is down to less than 0.1 PgCa^{-1} .

The strong reduction of the uncertainty estimate in the North America fluxes of TM5-4DVar in the “2/cont” run, despite assimilating only 2 sites in North America, shows the sensitivity of these estimates to the raw number of assimilated observations. It proves that the actual structure of the observations has to be taken into account when interpreting the reduction of model-estimated uncertainty.

Overall our results show that the current observation coverage in North America allows estimating robust fluxes on continental scales and on the scales of transcom regions. The historically improving agreement between both models for the aggregated North American fluxes and the two transcom regions in North America suggests that increasing the observation coverage allows getting robust fluxes on even smaller scales.

6 Conclusions

Our study evaluates the performance of the data assimilation models CarbonTracker and TM5-4DVar by comparing their a posteriori CO_2 concentration fields to measurements and by comparing their a posteriori surface fluxes. We test the sensitivity of the a posteriori CO_2 fluxes to model parameters and data coverage. To analyze the impact of the inverse method and the flux representation, the models run in setups which are close to their production settings but use harmonized input data, tracer transport model and prior estimates.

Both inverse models yield CO_2 concentration fields of comparable quality. We show that increasing the length of the assimilation time window of CarbonTracker to five bins of twenty days or ten bins of seven days gives a good agreement to observations in Antarctica which are underestimated in summer when using the default setup with an assimilation window of only five weeks. With these longer windows, the difference of the

CarbonTracker and TM5-4DVar

A. Babenhauserheide et al.

Title Page

Abstract

Introduction

Conclusions

References

Tables

Figures



Back

Close

Full Screen / Esc

Printer-friendly Version

Interactive Discussion



scale when only considering the uncertainty from the inverse methods and the flux representation.

**The Supplement related to this article is available online at
doi:10.5194/acpd-15-8883-2015-supplement.**

5 *Acknowledgements.* André Butz and Arne Babenhauserheide are supported by the Emmy-Noether program of the Deutsche Forschungsgemeinschaft (DFG) through grant BU2599/1-1 (RemoteC). This study would not have been possible without the work of Maarten Krol (SRON Netherlands Institute for Space Research, Utrecht, the Netherlands; Institute for Marine and Atmospheric Research (IMAU), Utrecht University, Utrecht, the Netherlands; Department of Meteorology and Air Quality (MAQ), Wageningen University and Research Centre, Wageningen, the Netherlands) who maintains the Transport Model 5 (TM5). Also the authors are indebted to the many individuals and institutions who have contributed original data to the ObsPack project, specifically version v1.0.2 2013-01-28 used in this study. They are J. A. Morgui (IC3); Ernst Brunke (SAWS); Samuel Hammer (UHEI-IUP); Shuji Aoki (NIPR); Markus Leuenberger (KUP); Harro Meijer (RUG); Hidekazu Matsueda (NIES-MRI); Juha Hatakka (FMI); Paul Krummel (CSIRO); Marcel van der Schoot (CSIRO); Margaret Torn (LBNL); Michel Ramonet (LSCE/RAMCES); Doug Worthy (EC); Angel J. Gomez-Pelaez (AEMET); Takakiyo Nakazawa (NIPR); Shinji Morimoto (NIPR); Luciana V. Gatti (IPEN); Ken Masarie (NOAA); Arlyn Andrews (NOAA); Ray Langenfelds (CSIRO); Sebastien Biraud (LBNL); Colm Sweeney (NOAA); Britton Stephens (NCAR); Paul Steele (CSIRO); Ed Dlugokencky (NOAA); Ralph Keeling (SIO); Eckhart Scheel (SAWS); Toshinobu Machida (NIES-MRI); Tuula Aalto (FMI); Hiroshi Koide (JMA); Steve Wofsy (HU); Martina Schmidt (LSCE/RAMCES); Yousuke Sawa (NIES-MRI); Laszlo Haszpra (HMS); Ingeborg Levin (UHEI-IUP); Kirk Thoning (NOAA); Casper Labuschagne (SAWS) and Pieter Tans (NOAA). Also we thank the CarbonTracker NOAA ESRL, Boulder, Colorado, USA for providing the 2011_oi results and documentation. Finally we thank Paul Tol from SRON for his work on colorschemes which work for colorblind people, O. Tange for easy ways to save time using GNU parallel and E. Jones and J. D. Hunter for their tools for convenient data analysis with Python.

Title Page

Abstract

Introduction

Conclusions

References

Tables

Figures



Back

Close

Full Screen / Esc

Printer-friendly Version

Interactive Discussion



The article processing charges for this open-access publication have been covered by a Research Centre of the Helmholtz Association.

References

- 5 Basu, S., Guerlet, S., Butz, A., Houweling, S., Hasekamp, O., Aben, I., Krummel, P., Steele, P., Langenfelds, R., Torn, M., Biraud, S., Stephens, B., Andrews, A., and Worthy, D.: Global CO₂ fluxes estimated from GOSAT retrievals of total column CO₂, *Atmos. Chem. Phys.*, 13, 8695–8717, doi:10.5194/acp-13-8695-2013, 2013. 8887, 8894, 8895, 8903, 8904, 8926
- 10 Bergamaschi, P., Krol, M., Meirink, J. F., Dentener, F., Segers, A., van Aardenne, J., Monni, S., Vermeulen, A. T., Schmidt, M., Ramonet, M., Yver, C., Meinhardt, F., Nisbet, E. G., Fisher, R. E., O'Doherty, S., and Dlugokencky, E. J.: Inverse modeling of European CH₄ emissions 2001–2006, *J. Geophys. Res.-Atmos.*, 115, D22309, doi:10.1029/2010JD014180, 2010. 8887
- 15 Bruhwiler, L. M. P., Michalak, A. M., Peters, W., Baker, D. F., and Tans, P.: An improved Kalman Smoother for atmospheric inversions, *Atmos. Chem. Phys.*, 5, 2691–2702, doi:10.5194/acp-5-2691-2005, 2005. 8907
- Bruhwiler, L. M. P., Michalak, A. M., and Tans, P. P.: Spatial and temporal resolution of carbon flux estimates for 1983–2002, *Biogeosciences*, 8, 1309–1331, doi:10.5194/bg-8-1309-2011, 2011. 8907
- 20 Chatterjee, A. and Michalak, A. M.: Technical Note: Comparison of ensemble Kalman filter and variational approaches for CO₂ data assimilation, *Atmos. Chem. Phys.*, 13, 11643–11660, doi:10.5194/acp-13-11643-2013, 2013. 8886, 8903
- Chevallier, F., Fisher, M., Peylin, P., Serrar, S., Bousquet, P., Bréon, F.-M., Chédin, A., and Ciais, P.: Inferring CO₂ sources and sinks from satellite observations: method and application to TOVS data, *J. Geophys. Res.*, 110, 24309, doi:10.1029/2005JD006390, 2005. 8893
- 25 Chevallier, F., Ciais, P., Conway, T. J., Aalto, T., Anderson, B. E., Bousquet, P., Brunke, E. G., Ciattaglia, L., Esaki, Y., Fröhlich, M., Gomez, A., Gomez-Pelaez, A. J., Haszpra, L., Krummel, P. B., Langenfelds, R. L., Leuenberger, M., Machida, T., Maignan, F., Matsueda, H., Morguí, J. A., Mukai, H., Nakazawa, T., Peylin, P., Ramonet, M., Rivier, L., Sawa, Y., Schmidt, M., Steele, L. P., Vay, S. A., Vermeulen, A. T., Wofsy, S., and Worthy, D.: CO₂
- 30

errors using TCCON measurements, *Atmos. Chem. Phys.*, 14, 3991–4012, doi:10.5194/acp-14-3991-2014, 2014. 8887

Jacobson, A. R., Mikaloff Fletcher, S. E., Gruber, N., Sarmiento, J. L., and Gloor, M.: A joint atmosphere–ocean inversion for surface fluxes of carbon dioxide: 2. Regional results, *Global Biogeochem. Cy.*, 21, GB1020, doi:10.1029/2006GB002703, 2007a. 8893

Jacobson, A. R., Mikaloff Fletcher, S. E., Gruber, N., Sarmiento, J. L., and Gloor, M.: A joint atmosphere–ocean inversion for surface fluxes of carbon dioxide: 1. Methods and global-scale fluxes, *Global Biogeochem. Cy.*, 21, B1019, doi:10.1029/2005GB002556, 2007b. 8892

Juhász, Z. and Bölöni, G.: Tests with the CONGRAD minimization algorithm within the ALADIN/HU 3DVAR system, congrad requires about 2/3rds of the CPU time required by M1QN3, University of Eötvös Loránd and Hungarian Meteorological Service (HMS), available at http://www.rclace.eu/File/Data_Assimilation/2007/jz_bg_congrad.pdf (last access: 20 March 2015), 2007. 8886

Kalnay, E.: The Future of Data Assimilation: 4D-Var or Ensemble Kalman Filter?, Talk at SAMSI, available at: <https://web.archive.org/web/20120915073405/http://www.atmos.umd.edu/~ekalnay/4DVarEnKFKalnaySAMSI.ppt.pdf> (last access: 20 March 2015), 2005. 8886

Krol, M., Houweling, S., Bregman, B., van den Broek, M., Segers, A., van Velthoven, P., Peters, W., Dentener, F., and Bergamaschi, P.: The two-way nested global chemistry-transport zoom model TM5: algorithm and applications, *Atmos. Chem. Phys.*, 5, 417–432, doi:10.5194/acp-5-417-2005, 2005. 8887, 8895

Lahoz, W. A. and Schneider, P.: Data assimilation: making sense of earth observation, *Frontiers in Environmental Science*, 2, 16, doi:10.3389/fenvs.2014.00016, 2014. 8885

Lahoz, W. A., Errera, Q., Swinbank, R., and Fonteyn, D.: Data assimilation of stratospheric constituents: a review, *Atmos. Chem. Phys.*, 7, 5745–5773, doi:10.5194/acp-7-5745-2007, 2007. 8885

Lanczos, C.: An iteration method for the solution of the eigenvalue problem of linear differential and integral operators, *J. Res. Nat. Bur. Stand.*, 45, 255–282, 1950. 8893

Masarie, K. A., Peters, W., Jacobson, A. R., and Tans, P. P.: ObsPack: a framework for the preparation, delivery, and attribution of atmospheric greenhouse gas measurements, *Earth Syst. Sci. Data*, 6, 375–384, doi:10.5194/essd-6-375-2014, 2014. 8897

Meesters, A. G. C. A., Tolk, L. F., Peters, W., Hutjes, R. W. A., Vellinga, O. S., Elbers, J. A., Vermeulen, A. T., van der Laan, S., Neubert, R. E. M., Meijer, H. A. J., and Dolman, A. J.:

ACPD

15, 8883–8932, 2015

CarbonTracker and TM5-4DVar

A. Babenhauserheide
et al.

Title Page

Abstract

Introduction

Conclusions

References

Tables

Figures



Back

Close

Full Screen / Esc

Printer-friendly Version

Interactive Discussion



CarbonTracker and
TM5-4DVarA. Babenhauserheide
et al.

Title Page

Abstract

Introduction

Conclusions

References

Tables

Figures



Back

Close

Full Screen / Esc

Printer-friendly Version

Interactive Discussion



Inverse carbon dioxide flux estimates for the Netherlands, *J. Geophys. Res.-Atmos.*, 117, D20306, doi:10.1029/2012JD017797, 2012. 8887

Meirink, J. F., Bergamaschi, P., and Krol, M. C.: Four-dimensional variational data assimilation for inverse modelling of atmospheric methane emissions: method and comparison with synthesis inversion, *Atmos. Chem. Phys.*, 8, 6341–6353, doi:10.5194/acp-8-6341-2008, 2008. 8887, 8893

Navon, I. M. and Legler, D. M.: Conjugate-gradient methods for large-scale minimization, in meteorology, *Mon. Weather Rev.*, 115, 1479–1502, 1990. 8893

NOAA Environmental Sciences Division, Oak Ridge National Laboratory: obspack CO₂ 1 PRO-TOTYPE v1.0.4 2013-11-25, doi:10.3334/OBSPACK/1001, 2013. 8886, 8897, 8928

Olson, J., Watts, J., and Allsion, L.: Major World Ecosystem Complexes Ranked by Carbon in Live Vegetation: a Database, Tech. rep., Carbon Dioxide Information Analysis Center, U.S. Department of Energy, Oak Ridge National Laboratory, Oak Ridge, Tennessee, USA, doi:10.3334/CDIAC/lue.ndp017, 1992. 8892

Peters, G. P., Andrew, R. M., Boden, T., Canadell, J. G., Ciais, P., Le Quere, C., Marland, G., Raupach, M. R., and Wilson, C.: The challenge to keep global warming below 2 °C, *Nature Climate Change*, 3, 4–6, doi:10.1038/nclimate1783, 2013. 8885

Peters, W., Miller, J. B., Whitaker, J., Denning, A. S., Hirsch, A., Krol, M. C., Zupanski, D., Bruhwiler, L., and Tans, P. P.: An ensemble data assimilation system to estimate CO₂ surface fluxes from atmospheric trace gas observations, *J. Geophys. Res.-Atmos.*, 110, 24304, doi:10.1029/2005JD006157, 2005. 8889, 8890, 8891, 8903

Peters, W., Jacobson, A. R., Sweeney, C., Andrews, A. E., Conway, T. J., Masarie, K., Miller, J. B., Bruhwiler, L. M. P., Pétron, G., Hirsch, A. I., Worthy, D. E. J., van der Werf, G. R., Randerson, J. T., Wennberg, P. O., Krol, M. C., and Tans, P. P.: An atmospheric perspective on North American carbon dioxide exchange: CarbonTracker, *P. Natl. Acad. Sci. USA*, 104, 18925–18930, doi:10.1073/pnas.0708986104, 2007. 8885, 8886, 8887, 8892, 8893, 8895, 8896, 8904

Peters, W., Krol, M. C., van der Werf, G. R., Houweling, S., Jones, C. D., Hughes, J., Schaefer, K., Masarie, K. A., Jacobson, A. R., Miller, J. B., Cho, C. H., Ramonet, M., Schmidt, M., Ciattaglia, L., Apadula, F., Heltai, D., Meinhardt, F., di Sarra, A. G., Piacentino, S., Sferlazzo, D., Aalto, T., Hatakka, J., Ström, J., Haszpra, L., Meijer, H. A. J., van der Laan, S., Neubert, R. E. M., Jordan, A., Rodó, X., Morguí, J.-A., Vermeulen, A. T., Popa, E., Rozanski, K., Zimnoch, M., Manning, A. C., Leuenberger, M., Uglietti, C., Dolman, A. J., Ciais, P.,

CarbonTracker and
TM5-4DVarA. Babenhauserheide
et al.

Title Page

Abstract

Introduction

Conclusions

References

Tables

Figures



Back

Close

Full Screen / Esc

Printer-friendly Version

Interactive Discussion



Heimann, M., and Tans, P. P.: Seven years of recent European net terrestrial carbon dioxide exchange constrained by atmospheric observations, *Glob. Change Biol.*, 16, 1317–1337, doi:10.1111/j.1365-2486.2009.02078.x, 2010. 8887

Peylin, P., Law, R. M., Gurney, K. R., Chevallier, F., Jacobson, A. R., Maki, T., Niwa, Y., Patra, P. K., Peters, W., Rayner, P. J., Rödenbeck, C., van der Laan-Luijkx, I. T., and Zhang, X.: Global atmospheric carbon budget: results from an ensemble of atmospheric CO₂ inversions, *Biogeosciences*, 10, 6699–6720, doi:10.5194/bg-10-6699-2013, 2013. 8885, 8887

Rodgers, C. D.: *Inverse Methods for Atmospheric Sounding: Theory and Practice* (Series on Atmospheric Oceanic and Planetary Physics), World Scientific Publishing Company, available at: <http://www.worldcat.org/isbn/981022740X> (last access: 20 March 2015), 2000. 8885, 8889

Schaefer, K., Collatz, G. J., Tans, P., Denning, A. S., Baker, I., Berry, J., Prihodko, L., Suits, N., and Philpott, A.: Combined Simple Biosphere/Carnegie-Ames-Stanford Approach terrestrial carbon cycle model, *J. Geophys. Res.-Biogeo.*, 113, G03034, doi:10.1029/2007JG000603, 2008. 8896

Schimel, D.: Carbon cycle conundrums, *P. Natl. Acad. Sci. USA*, 104, 18353–18354, doi:10.1073/pnas.0709331104, 2007. 8885

Schulze, E. D., Luyssaert, S., Ciais, P., Freibauer, A., Janssens, I. A., Soussana, J. F., Smith, P., Grace, J., Levin, I., Thiruchittampalam, B., Heimann, M., Dolman, A. J., Valentini, R., Bousquet, P., Peylin, P., Peters, W., Rödenbeck, C., Etiope, G., Vuichard, N., Wattenbach, M., Nabuurs, G. J., Poussi, Z., Nieschulze, J., Gash, J. H., and the CarboEurope Team: importance of methane and nitrous oxide for Europe's terrestrial greenhouse-gas balance, *Nat. Geosci.*, 2, 842–850, doi:10.1038/ngeo686, 2009. 8887

Skachko, S., Errera, Q., Ménard, R., Christophe, Y., and Chabrilat, S.: Comparison of the ensemble Kalman filter and 4D-Var assimilation methods using a stratospheric tracer transport model, *Geosci. Model Dev.*, 7, 1451–1465, doi:10.5194/gmd-7-1451-2014, 2014. 8886

Stocker, T. F., Dahe, Q., and Plattner, G.-K.: *Climate Change 2013: The Physical Science Basis*, Working Group I Contribution to the Fifth Assessment Report of the Intergovernmental Panel on Climate Change, Summary for Policymakers (IPCC, 2013), IPCC Working Group I Technical Support Unit, University of Bern, Bern, Switzerland, 2013. 8885

Thompson, R. L., Ishijima, K., Saikawa, E., Corazza, M., Karstens, U., Patra, P. K., Bergamaschi, P., Chevallier, F., Dlugokencky, E., Prinn, R. G., Weiss, R. F., O'Doherty, S., Fraser, P. J., Steele, L. P., Krummel, P. B., Vermeulen, A., Tohjima, Y., Jordan, A., Haszpra, L.,

CarbonTracker and
TM5-4DVarA. Babenhauserheide
et al.

Title Page

Abstract

Introduction

Conclusions

References

Tables

Figures



Back

Close

Full Screen / Esc

Printer-friendly Version

Interactive Discussion



Steinbacher, M., Van der Laan, S., Aalto, T., Meinhardt, F., Popa, M. E., Moncrieff, J., and Bousquet, P.: TransCom N₂O model inter-comparison – Part 2: Atmospheric inversion estimates of N₂O emissions, *Atmos. Chem. Phys.*, 14, 6177–6194, doi:10.5194/acp-14-6177-2014, 2014. 8887

5 Turner, A. J. and Jacob, D. J.: Balancing aggregation and smoothing errors in inverse models, *Atmos. Chem. Phys. Discuss.*, 15, 1001–1026, doi:10.5194/acpd-15-1001-2015, 2015. 8906

van der Velde, I. R., Miller, J. B., Schaefer, K., van der Werf, G. R., Krol, M. C., and Peters, W.: Terrestrial cycling of ¹³CO₂ by photosynthesis, respiration, and biomass burning in SiBCASA, *Biogeosciences*, 11, 6553–6571, doi:10.5194/bg-11-6553-2014, 2014. 8887

10 van der Werf, G. R., Randerson, J. T., Giglio, L., Collatz, G. J., Mu, M., Kasibhatla, P. S., Morton, D. C., DeFries, R. S., Jin, Y., and van Leeuwen, T. T.: Global fire emissions and the contribution of deforestation, savanna, forest, agricultural, and peat fires (1997–2009), *Atmos. Chem. Phys.*, 10, 11707–11735, doi:10.5194/acp-10-11707-2010, 2010. 8896

Whitaker, J. S. and Hamill, T. M.: Ensemble data assimilation without per-
15 turbed observations, *Mon. Weather Rev.*, 130, 1913–1924, doi:10.1175/1520-0493(2002)130<1913:EDAWPO>2.0.CO;2, 2002. 8886

Zhang, H. F., Chen, B. Z., van der Laan-Luijk, I. T., Machida, T., Matsueda, H., Sawa, Y., Fukuyama, Y., Langenfelds, R., van der Schoot, M., Xu, G., Yan, J. W., Cheng, M. L., Zhou, L. X., Tans, P. P., and Peters, W.: Estimating Asian terrestrial carbon fluxes from CON-
20 TRAIL aircraft and surface CO₂ observations for the period 2006–2010, *Atmos. Chem. Phys.*, 14, 5807–5824, doi:10.5194/acp-14-5807-2014, 2014. 8887

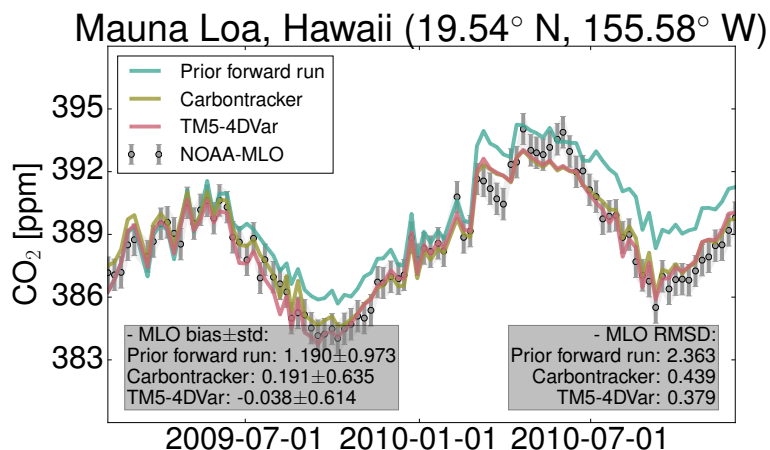
CarbonTracker and
TM5-4DVarA. Babenhausenheide
et al.

Figure 1. Time Series of measured and modelled CO₂ concentrations from CarbonTracker and TM5-4DVar at Mauna Loa, Hawaii, Pacific (assimilated weekly flasks), NOAA sitecode MLO. Also shown are the concentrations for obtained from a forward run of the transport model using the a priori background flux estimates.

Title Page

Abstract

Introduction

Conclusions

References

Tables

Figures



Back

Close

Full Screen / Esc

Printer-friendly Version

Interactive Discussion



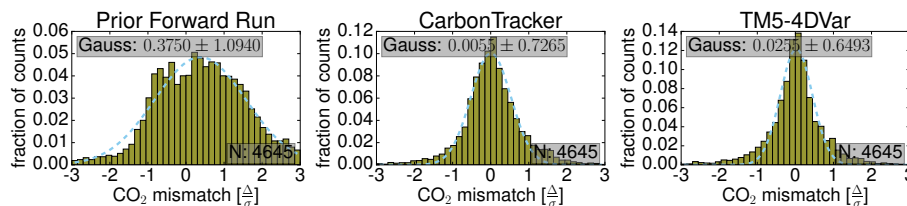
CarbonTracker and
TM5-4DVarA. Babenhausenheide
et al.

Figure 2. Histograms of the mismatch between measured and modelled CO_2 concentrations for all assimilated measurements using prior fluxes, CarbonTracker optimized fluxes and TM5-4DVar optimized fluxes. The histograms show residuals for one year (3 April 2009 to 2 April 2010) which are normalized by the estimated representativeness error. The line on top of the histograms is a fit of a Gauss function to the histogram. The parameters in the top left show the bias and standard deviation of the Gaussian. The bottom right shows the number of measurements which were accumulated into the histogram.

Title Page

Abstract

Introduction

Conclusions

References

Tables

Figures

◀

▶

◀

▶

Back

Close

Full Screen / Esc

Printer-friendly Version

Interactive Discussion



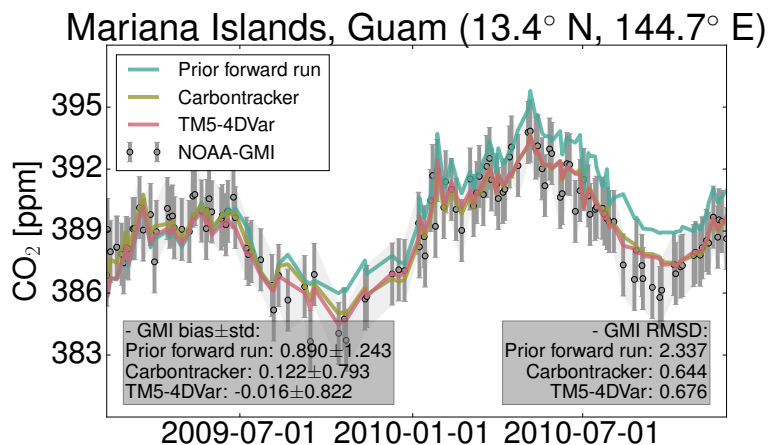
CarbonTracker and
TM5-4DVarA. Babenhausenheide
et al.

Figure 3. Time Series of measured and modelled CO₂ concentrations from CarbonTracker and TM5-4DVar at Guam, Mariana Islands, Pacific (non-assimilated). Also shown are the concentrations for obtained from a forward run of the transport model using the a priori background flux estimates.

Title Page

Abstract

Introduction

Conclusions

References

Tables

Figures



Back

Close

Full Screen / Esc

Printer-friendly Version

Interactive Discussion



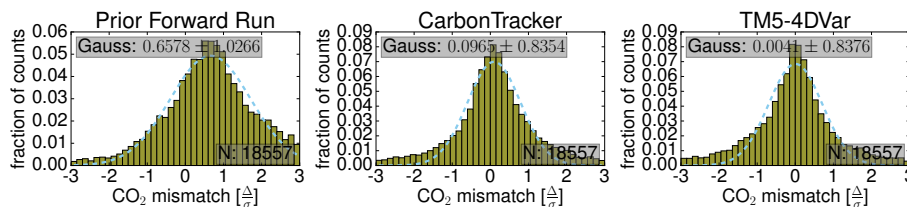
CarbonTracker and
TM5-4DVarA. Babenhausenheide
et al.

Figure 4. Histograms of the mismatch between measured and modelled CO₂ concentrations for all non-assimilated samples using prior fluxes, CarbonTracker optimized fluxes and TM5-4DVar optimized fluxes. The histograms show residuals for one year (3 April 2009 to 2 April 2010) which are normalized by the estimated representativeness error. The line on top of the histograms is a fit of a Gauss function to the histogram. The parameters in the top left show the bias and standard deviation of the histogram. The bottom right shows the number of measurements which were accumulated into the histogram.

[Title Page](#)[Abstract](#)[Introduction](#)[Conclusions](#)[References](#)[Tables](#)[Figures](#)[Back](#)[Close](#)[Full Screen / Esc](#)[Printer-friendly Version](#)[Interactive Discussion](#)

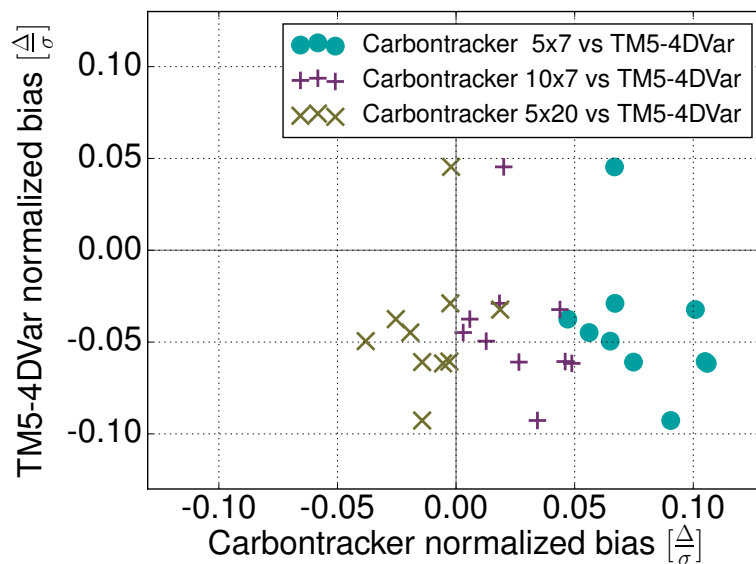
CarbonTracker and
TM5-4DVarA. Babenhausenheide
et al.

Figure 5. Model-measurement bias of TM5-4DVar against CarbonTracker for non-assimilated measurement sites. Each symbol corresponds to a case resampling exercise where the biases are calculated for 25 randomly drawn sites out of the total 50 resampling sites listed in Table 1 in the Supplement. The baseline run (dots) is compared to a CarbonTracker run with the assimilation period extended to 5×20 days (\times) instead of 5×7 days and 10×7 days ($+$).

Title Page

Abstract

Introduction

Conclusions

References

Tables

Figures



Back

Close

Full Screen / Esc

Printer-friendly Version

Interactive Discussion



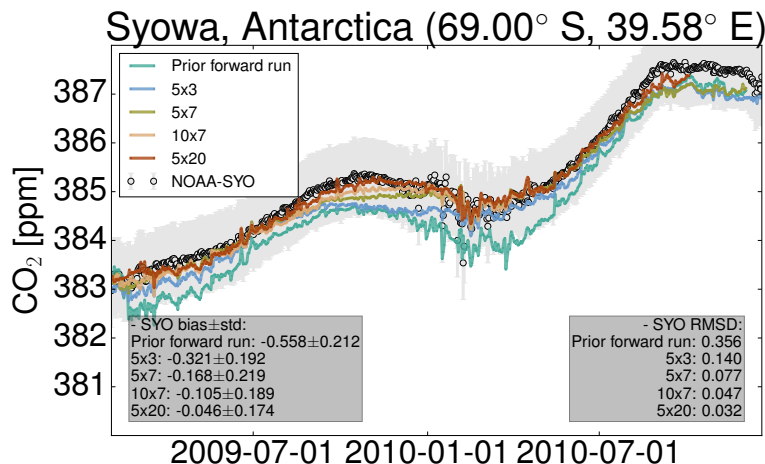
CarbonTracker and
TM5-4DVarA. Babenhausenheide
et al.

Figure 6. Time Series of measured and modelled CO_2 concentrations in Syowa, Antarctica, for CarbonTracker runs with different length of the assimilation time window. The baseline run uses an assimilation window of 5×7 days. Color coding of shorter and longer assimilation windows follows the legend (lag \times cycle in days).

Title Page

Abstract

Introduction

Conclusions

References

Tables

Figures



Back

Close

Full Screen / Esc

Printer-friendly Version

Interactive Discussion



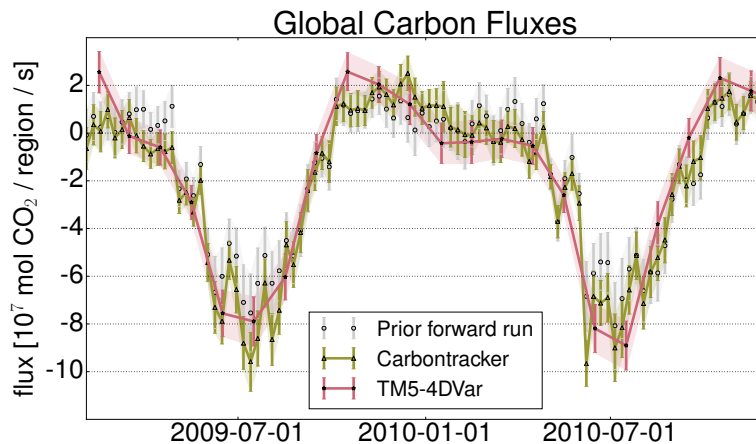
CarbonTracker and
TM5-4DVarA. Babenhausenheide
et al.

Figure 7. Global fluxes from the baseline runs of TM5-4DVar and CarbonTracker. The Prior is shown in the binning from CarbonTracker.

[Title Page](#)[Abstract](#)[Introduction](#)[Conclusions](#)[References](#)[Tables](#)[Figures](#)[◀](#)[▶](#)[◀](#)[▶](#)[Back](#)[Close](#)[Full Screen / Esc](#)[Printer-friendly Version](#)[Interactive Discussion](#)

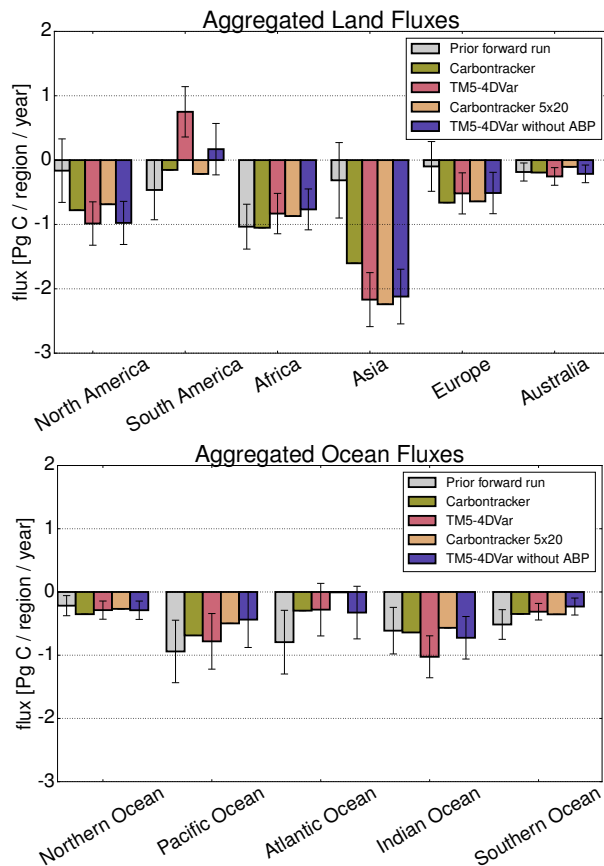
CarbonTracker and
TM5-4DVarA. Babenhausenheide
et al.

Figure 8. Fluxes from TM5-4DVar and Carbontracker aggregated on continental scale. The uncertainties for TM5-4DVar are calculated following Basu et al. (2013). The error bars for the prior are taken from TM5-4DVar. As written in Sect. 5.1 we show no uncertainties for CarbonTracker, because the aggregation of uncertainties from weekly to yearly scale is not clearly defined.

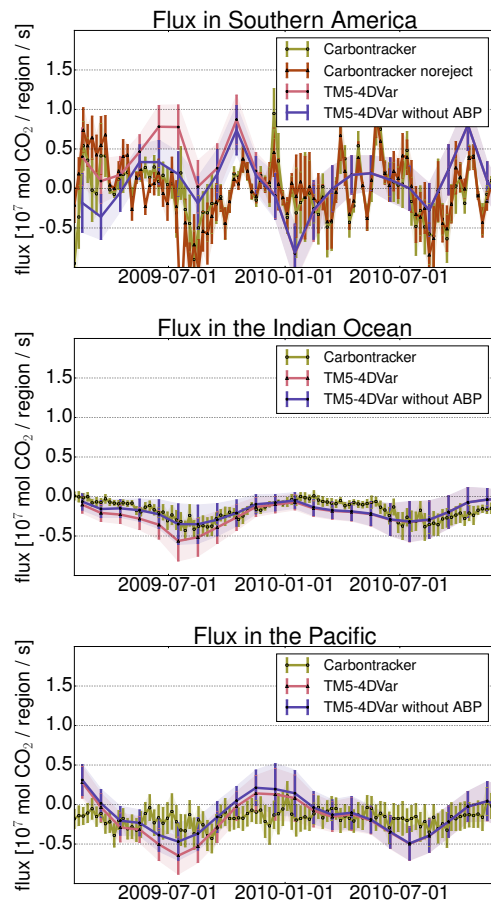
CarbonTracker and
TM5-4DVarA. Babenhausenheide
et al.

Figure 9. CO₂ surface fluxes from April 2009 to April 2010 in South America, the Indian Ocean and the Pacific. Only the timeseries for South America shows the CarbonTracker noreject, because it follows the CarbonTracker baseline in the other regions.

[Title Page](#)[Abstract](#)[Introduction](#)[Conclusions](#)[References](#)[Tables](#)[Figures](#)[Back](#)[Close](#)[Full Screen / Esc](#)[Printer-friendly Version](#)[Interactive Discussion](#)

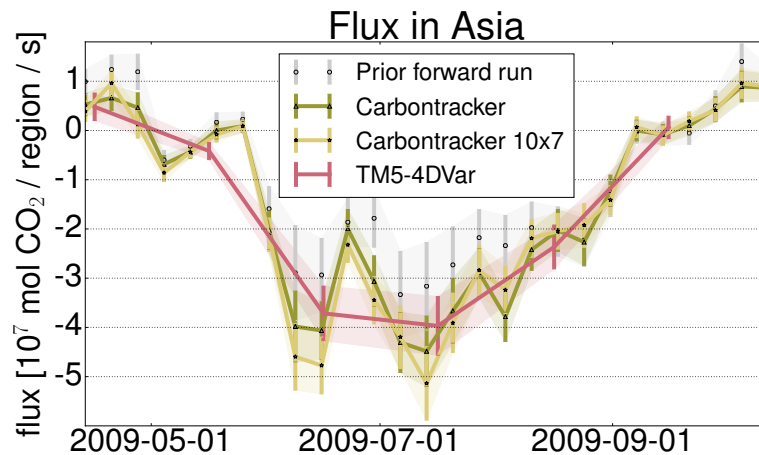
CarbonTracker and
TM5-4DVarA. Babenhausenheide
et al.

Figure 11. CO_2 surface fluxes during summer 2009 in Asia. The Prior Forward Run shows the prior fluxes aggregated to the binsize of the weekly Carbontracker scaling factors.

[Title Page](#)[Abstract](#)[Introduction](#)[Conclusions](#)[References](#)[Tables](#)[Figures](#)[◀](#)[▶](#)[◀](#)[▶](#)[Back](#)[Close](#)[Full Screen / Esc](#)[Printer-friendly Version](#)[Interactive Discussion](#)

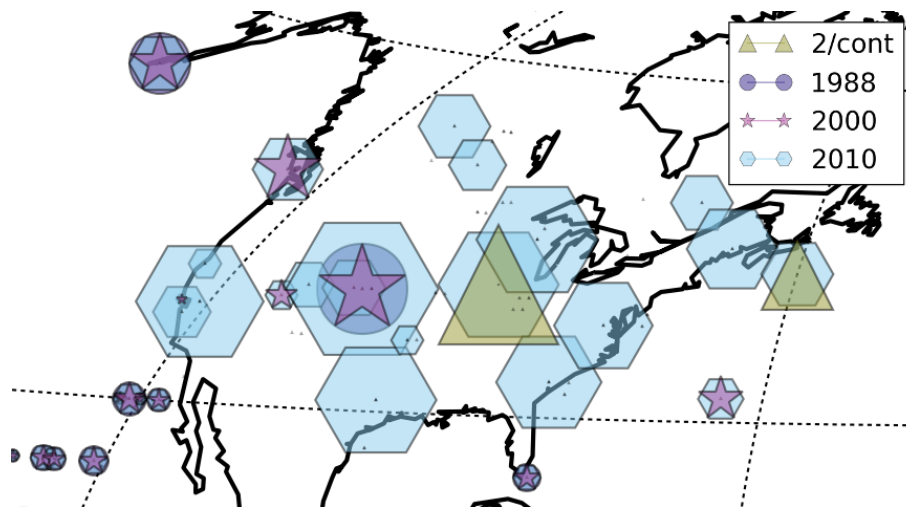
CarbonTracker and
TM5-4DVarA. Babenhauserheide
et al.

Figure 14. Visualization of the weight of the measurement sites which are assimilated in North America in the respective runs.

[Title Page](#)[Abstract](#)[Introduction](#)[Conclusions](#)[References](#)[Tables](#)[Figures](#)[◀](#)[▶](#)[◀](#)[▶](#)[Back](#)[Close](#)[Full Screen / Esc](#)[Printer-friendly Version](#)[Interactive Discussion](#)